Systems/Circuits

Thalamocortical mGlu8 Modulates Dorsal Thalamus Excitatory Transmission and Sensorimotor Activity

Bretton P. Nabit,[1,2] Anne Taylor,[2,3] and Danny G. Winder[1,2,3,4,5]

[1]Department of Pharmacology, [2]Vanderbilt Center for Addiction Research, [3]Vanderbilt Brain Institute, [4]Molecular Physiology and Biophysics, Vanderbilt University, Nashville, Tennessee 37203 and [5]Department of Neurobiology, University of Massachusetts Chan Medical School, Worcester, Massachusetts 01655

Metabotropic glutamate receptor 8 (mGlu8) is a heterogeneously expressed and poorly understood glutamate receptor with potential pharmacological significance. The thalamic reticular nucleus (TRN) is a critical inhibitory modulator of the thalamocortical–corticothalamic (TC–CT) network and plays a crucial role in information processing throughout the brain, is implicated in a variety of psychiatric conditions, and is also a site of significant mGlu8 expression. Using both male and female mice, we determined via fluorescent in situ hybridization that parvalbumin-expressing cells in the TRN core and shell matrices (identified by *spp1*+ and *ecel1*+ expression, respectively), as well as the cortical layers involved in CT signaling, express *grm8* mRNA. We then assayed the physiological and behavioral impacts of perturbing *grm8* signaling in the TC circuit through conditional (adeno-associated virus-CRE mediated) and cell-type-specific constitutive deletion strategies. We show that constitutive parvalbumin *grm8* knock-out (PV^{grm8} knock-out) mice exhibited (1) increased spontaneous excitatory drive onto dorsal thalamus relay cells and (2) impaired sensorimotor gating, measured via paired-pulse inhibition, but observed no differences in locomotion and thigmotaxis in repeated bouts of open field test (OFT). Conversely, we observed hyperlocomotive phenotypes and anxiolytic effects of AAV-mediated conditional knockdown of *grm8* in the TRN (TRN^{grm8} knockdown) in repeated OFT. Our findings underscore a role for mGlu8 in regulating excitatory neurotransmission as well as anxiety-related locomotor behavior and sensorimotor gating, revealing potential therapeutic applications for various neuropsychiatric disorders and guiding future research endeavors into mGlu8 signaling and TRN function.

Key words: **electrophysiology; mGlu receptor; mGlu8; sensorimotor gating; thalamic reticular nucleus; thalamocortical system**

Significance Statement

Group III metabotropic glutamate receptors and the thalamic reticular nucleus (TRN) are critical modulators of reciprocal corticothalamic neurotransmission and are implicated in anxiety and locomotor behaviors. The present study demonstrates a specific enrichment of *grm8* mRNA within the TRN and thalamus-projecting cortical layers and characterizes the role of mGlu8 receptors in controlling spontaneous excitatory neurotransmission onto cells located within the dorsal thalamus and regulating sensorimotor behaviors from open field and paired-pulse inhibition testing. These findings add to the growing bodies of literature regarding both TRN and *grm8* regulation of thalamocortical activity and related behaviors implicated in neurological and neuropsychiatric disorders.

Received Dec. 11, 2023; revised Feb. 25, 2024; accepted April 4, 2024.

Author contributions: B.P.N. and D.G.W. designed research; B.P.N. and A.T. performed research; B.P.N., A.T., and D.G.W. analyzed data; B.P.N. wrote the paper.

This research was supported by the National Institute on Drug Abuse 5R01DA042475 (D.G.W.). B.P.N. was supported by the National Institute on Drug Abuse F31DA05477. Imaging experiments were performed through the use of the Vanderbilt Cell Imaging Shared Resource. Behavioral analyses were performed through the use of the Murine Neurobehavioral Core Laboratory at the Vanderbilt University Medical Center. We thank John Allison, PhD, for his technical and managerial assistance and the Wellcome Trust Sanger Institute Mouse Genetics Project and its funders for providing the mutant mouse line C57BL/6N-A^{tm1Brd} $Grm8^{tm2a}$(KOMP)$^{Wtsi/WtsiH}$ and INFRAFRONTIER/EMMA (www.infrafrontier.eu). Funding information may be found at www.sanger.ac.uk.mouseportal and associated primary phenotypic information at www.mousephenotype.org.

The authors declare no competing financial interests.

Correspondence should be addressed to Danny G. Winder at danny.winder@umassmed.edu.

https://doi.org/10.1523/JNEUROSCI.0119-24.2024

Introduction

Disordered sensory perception is a common hallmark of numerous neuropsychiatric diseases. While the cerebral cortex exerts inhibitory, top-down control of sensorimotor activity, descending thalamocortical–ascending corticothalamic (TC–CT) glutamate circuits are under the regulatory influence of the thalamic reticular nucleus (TRN). Disruptions in TRN function are implicated in a wide variety of neurological and neuropsychiatric diseases (Gerardo and Manuel, 2020), including schizophrenia (Ferrarelli and Tononi, 2011; Pratt and Morris, 2015; Steullet et al., 2018; Thankachan et al., 2019; El Khoueiry et al., 2022; X. Zhu et al., 2021), seizure activity (Gerardo and Manuel,

2020), anxiety and fear learning (John et al., 2016; Lee et al., 2019; Zikopoulos and Barbas, n.d.), and other motor-related conditions (Pratt and Morris, 2015; Gerardo and Manuel, 2020). Thus, uncovering the versatile nature of TRN functionality across neurological and neuropsychiatric conditions is of high importance.

Metabotropic glutamate (mGlu) receptors are well-established targets in the development of novel pharmacotherapies for neurobiological diseases and are organized into three families based on sequence homology, ligand selectivity, and G-protein subtype coupling (Niswender and Conn, 2010). Group III mGlu receptors are $G\alpha_i$-coupled and typically located at presynaptic sites to regulate neurotransmitter release by decreasing intracellular cAMP production and other signaling cascades (Niswender and Conn, 2010). Drugs targeting group III mGlu receptors (comprising mGlu4, 6, 7, and 8) have gained attention as potential treatments for anxiety disorders (Spooren et al., 2010; Raber and Duvoisin, 2015; Ferraguti, 2018). Human genetic studies have identified numerous associations between polymorphisms in the mGlu8-encoding gene, *grm8*, and a variety of behavioral and neurophysiological measures characterized by negative affect and externalizing behaviors (Gast et al., 2013; Long et al., 2015; Bauer and Covault, 2020), but we lack an understanding of *grm8* function in the discrete brain regions and neural circuits that are implicated in producing anxiety and externalizing behaviors, such as the TRN. *Grm8* is significantly enriched in the TRN (Saugstad et al., 1997) and cortical layers that participate in reciprocal TC communication and also expressed by inhibitory and excitatory cells (Marabese et al., 2005, 2007; Gosnell et al., 2011; Dobi et al., 2013; Mercier et al., 2013), suggesting a potential versatile function of mGlu8 signaling in both glutamatergic and GABAergic synaptic circuits. Preclinical studies in constitutive mGlu8 knock-out (KO) mice suggest that *grm8* regulates activity of stress-sensitive brain regions and produces related behaviors (Linden et al., 2002, 2003b), potentially through enhanced recruitment of the dorsal thalamus, which facilitates proper sensorimotor behaviors (Linden et al., 2003a).

Using a combination of fluorescent in situ hybridization, conditional allele-based knockdown (KD) strategies, whole-cell patch-clamp electrophysiology, and a variety of behavioral analyses, we demonstrate that the TRN and cortical layers that communicate with the dorsal thalamus are rich in *grm8*-expressing parvalbumin (PV) neurons, and disruption of *grm8* function on PV resulted in increased spontaneous excitatory drive onto thalamic relay cells that was associated with impaired sensorimotor gating in paired-pulse inhibition (PPI) assays, while conditional TRN-specific *grm8* KD (TRN^{grm8} KD) disrupted sensorimotor habituation, increased locomotion, and decreased anxiety measures in repeated bouts of open field test (OFT). Together, these findings suggest that *grm8* regulates synaptic transmission onto TC relay neurons and sensorimotor behaviors through the cortex and TRN-specific mechanisms and further highlights the importance of mGlu8 signaling in the TC system as a potential therapeutic target.

Materials and Methods

Animals

Male and female mice >8 weeks of age were used for this study. All mice were housed 2–5 per cage and maintained on a 12 h light/dark cycle (lights on 0600 through 1800 h) under controlled temperature (20–25°C) and humidity (30–50%). Water and food were available *ad libitum*. *Grm8* mice ($Grm8^{tm2a(KOMP)Wtsi}$, EMMA ID: EM:07403) were purchased from Wellcome Trust Sanger Institute Mouse Genetics Project (Pettitt et al., 2009; Skarnes et al., 2011; Bradley et al., 2012; White et al., 2013) and rederived at the Vanderbilt University Transgenic Mouse Core. Homozygous conditional *grm8* KO mice ($Grm8^{flx/flx}$) were generated by crossing F_1 generation of $Grm8^{tm2a}$ animals with transgenic, hemizygous FLP recombinase mice (JAX ID: 009086) and then recrossed to generate homozygous floxed animals ($Grm8^{flx/flx}$) as outlined by the Wellcome Trust Sanger Institute guidelines. Transgenic animals were bred in-house and genotyped through Transnetyx Genotyping Services. Animals were maintained on a C57BL/6J background and backcrossed as necessary.

For the molecular confirmation of *grm8* KO, homozygous $Grm8^{flx/flx}$ mice were crossed with female CMV-cre driver mice [B6.Tg(CMV-cre) 1Cgn/J; JAX: 006054] and then recrossed with homozygous floxed mice to produce constitutive *grm8* KO animals. The same breeding schema was used to generate PV^{grm8} KO animals utilizing PV-cre driver mice [B6;129P2-$Pvalb^{tm1(cre)Arbr}$/J; JAX: 008069]. All animal procedures were approved by the Vanderbilt University Institutional Animal Care and Use Committee (IACUC) and were carried out in accordance with the guidelines set in the Guide for the Care and Use of Laboratory Animals of the National Institutes of Health. All behavioral experimentation was carried out in the Vanderbilt Murine Neurobehavioral Core.

Stereotaxic surgeries

Adult mice (~8 weeks of age) were anesthetized with an initial 3% dose of isoflurane and maintained at 1.5%. Surgeries were performed with an Angle Two stereotaxic frame (Leica Microsystems) to intracranially inject adeno-associated virus (AAV) directly into the rostroventral TRN based on the Paxinos and Franklin 2004 mouse brain atlas (from the bregma: AP, −0.6 mm; ML, ±1.0 mm; DV, −4.0 mm; tilt, 21.96°) at a rate of 60–100 nl/min. For behavioral studies using the $Grm8^{flx/flx}$ line, animals received bilateral, 350 nl injections of recombinant AAV5-CMV-eGFP or AAV5-CMV-CRE-eGFP (UNC Vector Core) and given a minimum of 4 weeks to recover. Mice were treated with 5 mg/kg ketoprofen or 2.5 mg/kg Metacam for 48 h to facilitate postsurgery recovery. Genotyping was performed through Transnetyx. All surgical procedures were approved by the Vanderbilt University IACUC and were carried out in accordance with the guidelines set in the Guide for the Care and Use of Laboratory Animals of the National Institutes of Health.

Behavioral testing

Age- and sex-matched animals were used in all experiments. Behavioral experiments were always started in the morning (0700 h) at the beginning of the animal's light phase (Zeitgeber 1–Zeitgeber 2), and the experimenter wore nursing scrubs during behavioral procedures. Group-housed male and female $Grm8^{flx/flx}$ animals received intra-TRN injections of CMV-cre-gfp (TRN^{grm8} KD) or CMV-gfp-only control AAV vectors and then transferred to the Vanderbilt Murine Neurobehavioral Laboratory for a minimum of 3 weeks prior to testing, allowing for at least 1 week of acclimation and 1 week of handling acclimation immediately preceding testing. Animals were handled for 5 d as previously described to decrease potential experimenter-induced stress. On test days, mice were brought to and kept in the procedure rooms ~1 h prior to beginning of testing to allow for acclimation, during which animals had access to food and water *ad libitum*, and light intensity was kept high (~350–500 lux). All utilized equipment were cleaned with 70% ethanol solution before start and between each animal run in order to mask other scents and odors that could interfere with experimentation.

OFT. Mice were run in ENV-S10S open field activity chambers (Med Associates) that use IR photograph-beam arrays for 60 min in fully lit conditions (~350 lux). The total chamber area accessible to the mouse was 727 cm^2 (center zone, 362 cm^2; surround, 365 cm^2). Locomotor activity and zone analyses for time spent in the center versus surrounding areas were performed using the native Med Associates software. For OFT over multiple days, animals were always retested in the original chamber that they were tested in on Day 1.

Elevated zero maze (EZM). Subjects were placed onto the open arm of an EZM and tested for 5 min. Video recordings and behavioral analyses were performed with AnyMaze behavioral software (Stoelting). The apparatus was cleaned with 70% ethanol in-between subjects.

PPI. Subjects were placed into Med Associates PPI chambers with a ANL-925C amplifier prior to protocol start. Sixty-four trials were conducted at varied intertrial interval type and intertrial interval duration after a 5 min acclimation period with a constant 65 dB background noise throughout. Stimulus (120 dB) durations were 250 ms long, and prepulse were delivered 50 ms before the main stimulus. Startle curves were run without prepulse tones to assess basal startle levels.

mRNA isolation and qRT-PCR

Male and female animals were deeply anesthetized, and the brain was rapidly prepared into 0.5-mm-thick sections. Tissue punches were taken with 16-gauge syringe in ice-cold PBS and then rapidly frozen on dry ice and stored at −80°C until processing. mRNA isolation was performed via TRIzol reagent per the manufacturer's guidelines (https://assets.thermofisher.com/TFS-Assets/LSG/manuals/trizol_reagent.pdf), eluted in 30 µl RNase-free water and quantified via nanodrop. Prior to cDNA synthesis, RNA sample concentrations were equalized by diluting to match the least concentrated sample. cDNA synthesis was performed with the QuantiTect reverse transcription kit (Qiagen, catalog #205311) per the manufacturer's instructions. cDNA samples were again diluted at 1:5 prior to qPCR. RT-qPCR was performed in triplicates utilizing the SsoAdvanced Universal SYBR Green Supermix (Bio-Rad) on Bio-Rad CFX96 plate readers. Predesigned PrimeTime qPCR primer sets for reference genes *HPRT1* (Mm.PT.39a 22214828), *EAAT1* (Mm.PT.58.5217423), and *grm7* (Mm.PT.58.43156724) were purchased from Integrated DNA Technologies. Custom PrimeTime qPCR primer sets targeting the exon 3–exon 4 cDNA junction (forward, GATCTCAAGGGAGATTGG; reverse, GGCAAACATAATCACTGC) in wild-type *grm8* transcript (ENSMUSG00000024211) were designed with IDT's PrimerQuest design tool. Data were analyzed on CFX Maestro software from Bio-Rad.

Whole-cell patch-clamp electrophysiology

Mice were killed via isoflurane anesthesia and then were rapidly decapitated following intracardial perfusion with ice-cold preoxygenated (95%O_2/5% CO_2) NMDG-based slice buffer consisting of the following (in mM): 93 NMDG, 30 $NaHCO_3$, 25 glucose, 20 HEPES, 2.5 KCl, 1.2 NaH_2PO_4, 10 $MgCl_2$, 0.5 $CaCl_2$, 5 Na ascorbate, 3 Na pyruvate, 5 *N*-acetylcysteine, adjusted to pH 7.3–7.4 and 300–310 mOsm. Coronal slices (300 µm) containing the paraventricular thalamus were prepared from whole-brain tissue using a Vibratome (Leica VT1200S; Leica Instruments). Slices were then placed into a warm bath (32–34°) containing the same NMDG-based slice buffer for 10–15 min. Slices were then transferred to a chamber containing oxygenated artificial cerebrospinal fluid (ACSF; in mm): 119 NaCl, 2.5 KCl, 1.3 $MgCl_2$-$6H_2O$, 2.5 $CaCl_2$-$2H_2O$, 1.0 NaH_2PO_4-H_2O, 26.2 $NaHCO_3$, and 11 glucose, 287–295 mOsm), 298–302 mOsm, for 1 h at room temperature before recording.

All experiments were performed and analyzed with pClamp 11.1 (Molecular Devices). Recordings were made using a 10 kHz sampling rate and a 2 kHz low-pass filter. Slices were transferred to an interface recording chamber and continuously perfused with 28–32°C ACSF at 2 ml/min. The paraventricular nucleus of the thalamus (PVT) neurons were patched onto randomly and viewed with a halogen bulb. PVT cells were confirmed according to morphologic (size, shape) and biophysical properties (e.g., capacitance and membrane resistance) and patched with 3–5 MΩ recording pipettes (P-97 Micropipette Puller).

Voltage-clamp recordings were performed using a cesium-based internal solution (in mM): 140 $CsMeSO_3$, 5 NaCl, 10 HEPES, 0.2 EGTA, 2 MgATP, 0.2 NaGTP, and 5 QX-314, 310–315 mOsm. Cells were held at 0 mV to record spontaneous inhibitory postsynaptic currents (sIPSCs) and at −70 mV to record spontaneous excitatory postsynaptic currents (sEPSCs). Data were collected for 5 min at each membrane potential. A maximum of three cells per animal were collected for use in data analysis.

In situ hybridization (RNAscope)

Tissue was collected and prepared as previously described (Harris et al., 2018; Fetterly et al., 2019; Salimando et al., 2020), with minor alterations. The RNAscope Multiplex Fluorescent V2 assay kit was used to visualize single molecules of mRNA expressed by neurons within the TRN. Reagents were purchased from Advanced Cell Diagnostics and were applied to fresh-frozen tissue preparations. The probes directed against *pvalb* (catalog #421931; Channel 1), *grm8* (catalog #521491; Channel 2), *ecel1* (catalog #475331; Channel 3), and *spp1* (catalog #435191; c=Channel 3) were purchased from Advanced Cell Diagnostics and prepared at a 50:1:1 ratio (C1:C2:C3). C57BL/6J male and female mice, aged 7–10 weeks, were anesthetized with isoflurane, and the brains were quickly removed and frozen in Tissue Tek OCT compound (Sakura) and then stored at −80°C until being cut at 14-µm-thick coronal sections on a CM3000 cryostat (Leica Microsystems). Slices were directly mounted from cryostat to Fisher Plus Charged Slides and stored at −80°C until ready to undergo RNAscope staining.

In brief, slides were fixed for 15 min in ice-cold 4% PFA and then dehydrated in increasing ethanol serial dilutions (50%, 70%, 2× 100%). Slides were pretreated with ACD's Pretreat IV solution for ∼30 min in a humidified chamber at 40°C. Then, slides were incubated with mRNA probes for 2 h and then with a series of signal amplification reagents provided by ACD: Amp 1, Amp 2, and Amp 3. TSA vivid dyes were used as part of the V2 RNAscope workflow at a 1:1,500 working dilution following reconstitution with 100 µl DMSO. Channel 1 was visualized with TSA Vivid Dye 520 (FITC), Channel 2 with TSA Vivid Dye 570 (TRITC), and Channel 3 with TSA Vivid Dye 650 (Cy5). Finally, sections were counterstained with DAPI prior to application of Aqua-Poly Mount Media (Polysciences) and coverslips and then were allowed to dry in a cool, dark place. A minimum of one section was stained with a probe and another with a negative control probe that stains bacterial *dapB* mRNA (which is absent in mice).

Sections were imaged using an 880 scanning confocal microscope (Carl Zeiss). Composite images of the TRN were saved as TIF files and analyzed in Fiji/ImageJ with matching laser strength, gain, and pinhole size. Sections stained with a negative control probe were used to set parameters for laser settings and image brightness. Adjusted experimental images were analyzed with regions of interest (ROIs) containing the TRN. Cells in these ROIs were marked with DAPI-stained nuclei, and connecting nuclei were split apart by Fiji/ImageJ "watershed" function. Finally, the total number of cells in each region was counted with transcripts being readily identifiable as round punctate dots surrounding the DAPI-labeled nuclei.

Experimental design and statistical analyses

All data are represented as mean ± standard error of the mean. Data and plots were visualized using Prism 9 (GraphPad Software). Statistical tests (either Student's two-tailed *t* test or two-way RM-ANOVA) are noted where appropriate in each experimental section. Cell density measurements from in situ analyses were determined by using an ROI of ∼14 mm^2, and three separate replicate counts per region from one brain slice were averaged to represent one animal. Comparisons in behavior experiments with sex- and age-matched subjects were ran as two-way repeated measures ANOVA with Fisher's noncorrected LSD. To determine statistical significance, we compared our generated *p*-values from Prism9 to alpha values of 0.05 ($\alpha = 0.05$). Power analyses were performed with preliminary data, and previously ran experiments and papers were used to help determine proper sample sizes across groups. Analyses of sex as a biological variable were performed in all experiments, and data were represented as combined male and female averages unless there was a statistically significant difference in male versus female subjects.

Results

Grm8 is heavily expressed by PV+ interneuron populations located throughout the TC circuitry

Early studies on *grm8* identified a heterogenous expression pattern throughout the brain (Duvoisin et al., 1995; Saugstad et al., 1997), and recent snRNA-seq studies have identified *grm8*-positive cells within the TC system (Y. Li et al., 2020), but we lack in situ data with higher fidelity spatial information regarding subregion- and cell-type-specific *grm8* expression. Thus, we assayed *grm8* and several cell-type markers throughout the TC system. Perfused brains were rapidly collected and processed with RNAscope© V2 Multiplex system and subsequently imaged via confocal microscopy. *Grm8* expression was readily identified throughout the medial and midline dorsal thalamic nuclei at the level of the anterior third ventricle (Fig. 1*A*).

We observed strong *grm8* expression that delineated the border of the TRN and colocalized with PV expression (Fig. 1*B,C*). The PV cells that comprise the TRN, depending on their location within the TRN shell or core, project to higher-order and first-order thalamic neurons, respectively (Y. Li et al., 2020). Here, ∼80% of PV cells expressed *grm8* along the rostral–caudal axis of the TRN (Fig. 1*D*; coronal brain atlas images from the Allen Institute for Brain Science). Furthermore, we show that *grm8* is present on both the higher-order neuron-projecting *ecel1*+ "shell" cells and first-order neuron-projecting *spp1*+ "core" cells (Fig. 1*I*) at comparable cell densities and coexpression levels (Fig. 1*J*). The level of *spp1*+ *grm8*+ cells were slightly higher than the amount of *ecel1*+ *grm8*+ cells, but it remains that the findings suggest *grm8* is poised to regulate GABAergic synaptic activity onto first- and higher-order neurons in the dorsal thalamus.

Grm8 expression was noted throughout the somatosensory cortical layers—particularly in Layers II/III, V, and VI (Fig. 1*E*). In the cortex, PV cells play traditional interneuron roles to regulate the firing activity of pyramidal neurons (Nahar et al., 2021). Consistent with previous studies (Kawaguchi and Kubota, 1997), PV expression was scattered throughout the cortical layers. We sought to quantify PV expression in cortical layers that project to the TRN and thalamus, so ROIs were placed within Layers V and VI (Carroll et al., 2022). We identified region-dependent effects on cell densities, with significantly higher cell densities of *grm8*+ cells in the somatosensory cortex compared with the TRN, whereas in the TRN, we observed significantly increased densities of PV+ and *grm8*+ PV+ cells [Fig. 1*G*; effect of region, $F_{(1,18)} = 3.567$, $p = 0.0752$; effect of cell type, $F_{(2,18)} = 60.25$, $p < 0.0001$; region × cell-type interaction, $F_{(2,18)} = 55.34$, $p < 0.0001$]. Overall, there was higher prevalence of PV+ *grm8*+ cells in the TRN compared with the somatosensory cortex (Fig. 1*H*; two-tailed independent sample *t* test, $t_6 = 3.505$; $p = 0.0127$). Thus, we hypothesize that *grm8*+ PV+ cells in the TRN synapse directly onto other TRN neurons or thalamic relay neurons, while cortical *grm8*+ PV+ cells represent local inhibitory interneurons that may regulate the activity of thalamus-projecting pyramidal cells, representing multiple mechanisms by which *grm8* can regulate the TC system.

Derivation of $Grm8^{flx/flx}$ mouse line to assess brain region- and cell-type-specific *grm8* function

To date, studies identifying effects of constitutive *grm8* deletion on behavior and physiology have employed constitutive, body-wide KO lines. While practical to determine general target function, these models do not provide information regarding discrete cell-type- or brain region-specific functionality of *grm8* or any other heterogeneously expressed target. To circumvent this issue, we validated and employed a conditional KO (or, floxed, flx) approach with a novel *grm8* mouse line, $Grm8^{flx/flx}$, that we used to generate cell-type-specific and region-specific *grm8* mutations.

We first validated our model by crossing $grm8^{flx/flx}$ animals to hemizygous CMV-cre driver mice, producing constitutive *grm8* KO animals (Fig. 2*A*). Then, through qRT-PCR, we show decreased relative levels of *grm8* expression (compared with housekeeping gene *HPRT*) in brain regions known to be enriched for *grm8*, such as the TRN, the entorhinal cortex, and the dentate gyrus (Fig. 2*B–D*). We also assayed for and found no differences in relative expression levels of the excitatory amino acid transporter (*eatt1*) in the same regions, to determine if the *grm8* KO mice showed perturbed glutamate system homeostasis. After confirming, we investigated the role of *grm8* expressed by PV neurons in regulating neurotransmission and sensorimotor behaviors through the use of a PV-cre driver mouse line (Fig. 2*E*). We performed qRT-PCR in TRN samples from PV^{grm8} KO mice and observed decreased levels of *grm8* (Fig. 2*F*; Student's two-tailed *t* test, $t_{14} = 2.237$, $^*p = 0.0420$) but no changes in the expression of *grm7* levels (Fig. 2*F*; Student's two-tailed *t* test, $t_{14} = 0.5957$, $p = 0.5609$, ns), a known dimerization partner of mGlu8 (Lin et al., 2022).

PV^{grm8} KO enhanced excitatory transmission onto thalamic relay neurons

Nuclei in the dorsal thalamus receive inputs from both the cortex and TRN (Lam and Sherman, 2007; Wang et al., 2001; Mease and Gonzalez, 2021; S. H. Li et al., 2024). To elucidate the role of mGlu8 in regulating synaptic transmission within the TC system, we focused on the PVT, a hub for coordinating stress responses and salience-motivated behaviors via unique connectivity between the cortex and amygdala (James and Dayas, 2013; M. Chen and Bi, 2019; Green and Green, 2022; S. H. Li et al., 2024; S. Li and Kirouac, 2008; Penzo et al., 2015; Y. B. Zhu et al., 2022). Due to the high degree of colocalization of *grm8* and PV transcript observed in the TRN and cortex, and the projections regulated by or comprising PV+ cells in the cortex or TRN, we generated a PV-specific *grm8* KO model (PV^{grm8} KO; Fig. 3*A*) to determine the role of PV^{grm8} in regulating spontaneous excitatory and inhibitory postsynaptic currents (sEPSC, sIPSC) onto PVT cells. Cells were patched onto and excitatory and inhibitory spontaneous transmissions were measured in voltage-clamp mode.

We observed increased frequency of sEPSCs ($t_{22} = 3.735$, $^{**}p = 0.0011$; littermate control: 0.81 Hz ± 0.09 Hz vs PV^{grm8} KO: 1.58 Hz ± 0.1820 Hz), while the sEPSC amplitude was not significantly different across genotypes (Fig. 3*B*; $t_{22} = 1.503$, $p = 0.1471$, n.s.; littermate control: 13.08 pA ± 0.6263 pA vs PV^{grm8} KO: 15.10 pA ± 1.187 pA). We originally hypothesized that inhibitory transmission onto relay neurons would be increased in PV^{grm8} KO animals, as would be expected when removing mGlu8, a $G_{\alpha i}$-coupled presynaptic receptor, from GABA-releasing TRN terminals. Surprisingly, we observed no differences in sIPSC frequency (Fig. 3*C*; frequency: $t_{22} = 0.1861$, $p = 0.8541$, n.s.; littermate control: 1.691 Hz ± 0.1656 Hz vs PV^{grm8} KO: 1.738 Hz ± 0.1916 Hz) or amplitude (amplitude: $t_{22} = 0.9050$, $p = 0.3753$, n.s.; littermate control: 16.35 pA ± 1.740 pA vs PV^{grm8} KO: 14.58 pA ± 0.8843 pA) between mutant and control animals.

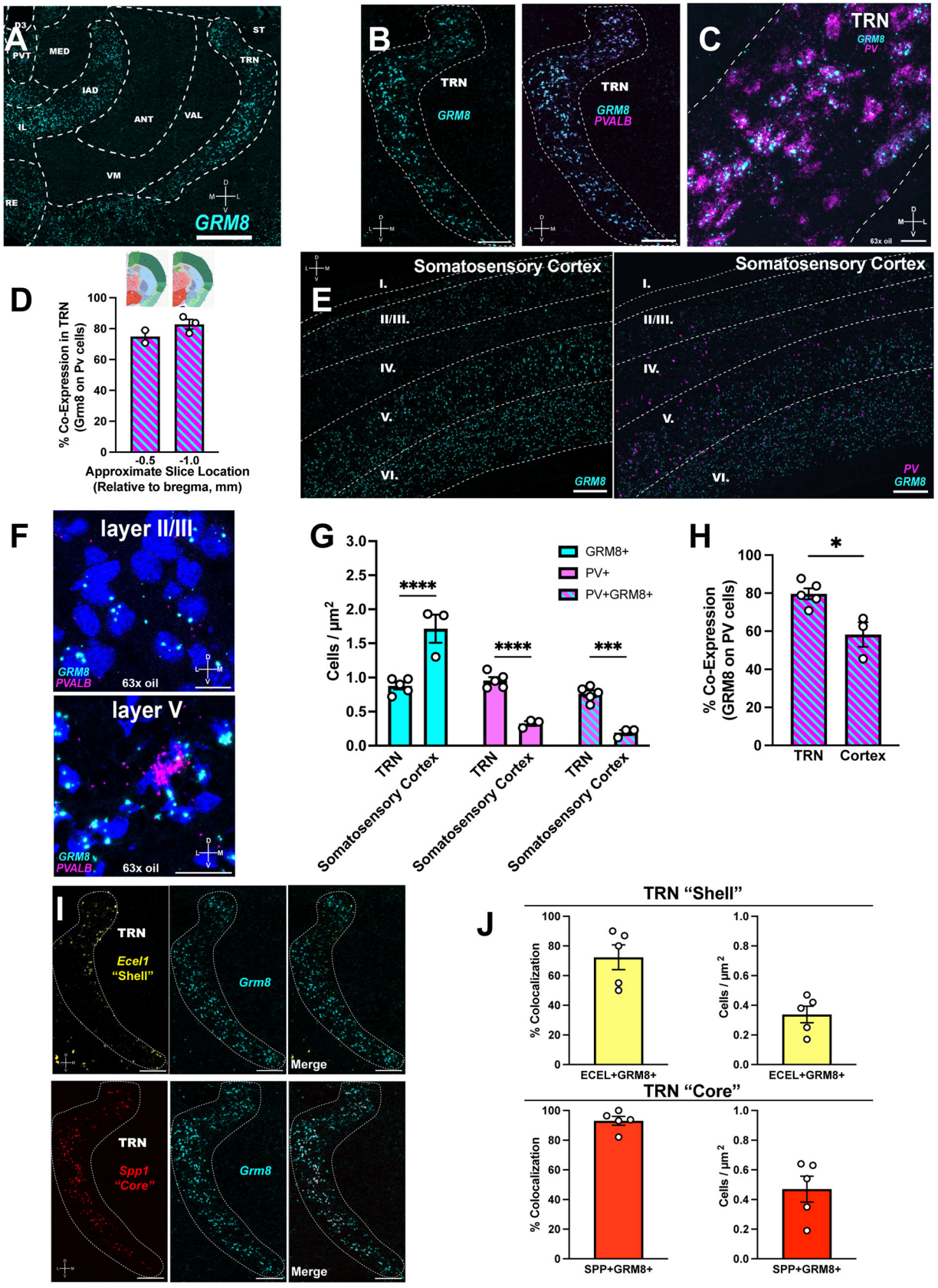

Figure 1. *Grm8* expression throughout thalamic nuclei that participate in TC transmission. ***A***, Representative image depicting strong labeling of *grm8* throughout the dorsal thalamus (***B***) *grm8* and PV mRNA expression in TRN. ***C***, A 63× oil immersion image of *grm8* and PV overlap in the TRN. ***D***, Levels of *grm8*+PV+ cells along the rostral–caudal axis of the TRN. Coronal slices are from Allen Institute Coronal Mouse Brain Atlas. ***E***, *Grm8* and PV staining in the primary somatosensory cortex layers at the level of the anterior third ventricle. ***F***, A 63× oil immersion image of dorsal and ventral cortical layers with differential *grm8*+PV+ coexpression. ***G***, Mixed effects comparison of *grm8*+, PV+, and colabeled cell densities in the TRN and cortex with Bonferroni post hoc analysis. ***H***, The TRN has slightly higher levels of *grm8*+PV+ cells compared with the cortex. ***I***, *Grm8* strongly associates with TRN "shell" (*ecel1*+) and "core" (*spp1*+) markers. ***J***, Cell densities and coexpression levels of *ecel1*+*grm8*+ and *spp1*+*grm8*+ cells. $N = 3–5$ mice where indicated. Scale bar = 200 µm (except in ***F***, scale bar = 50 µm; $****p < 0.0001$, $***p < 0.001$, $*p < 0.05$).

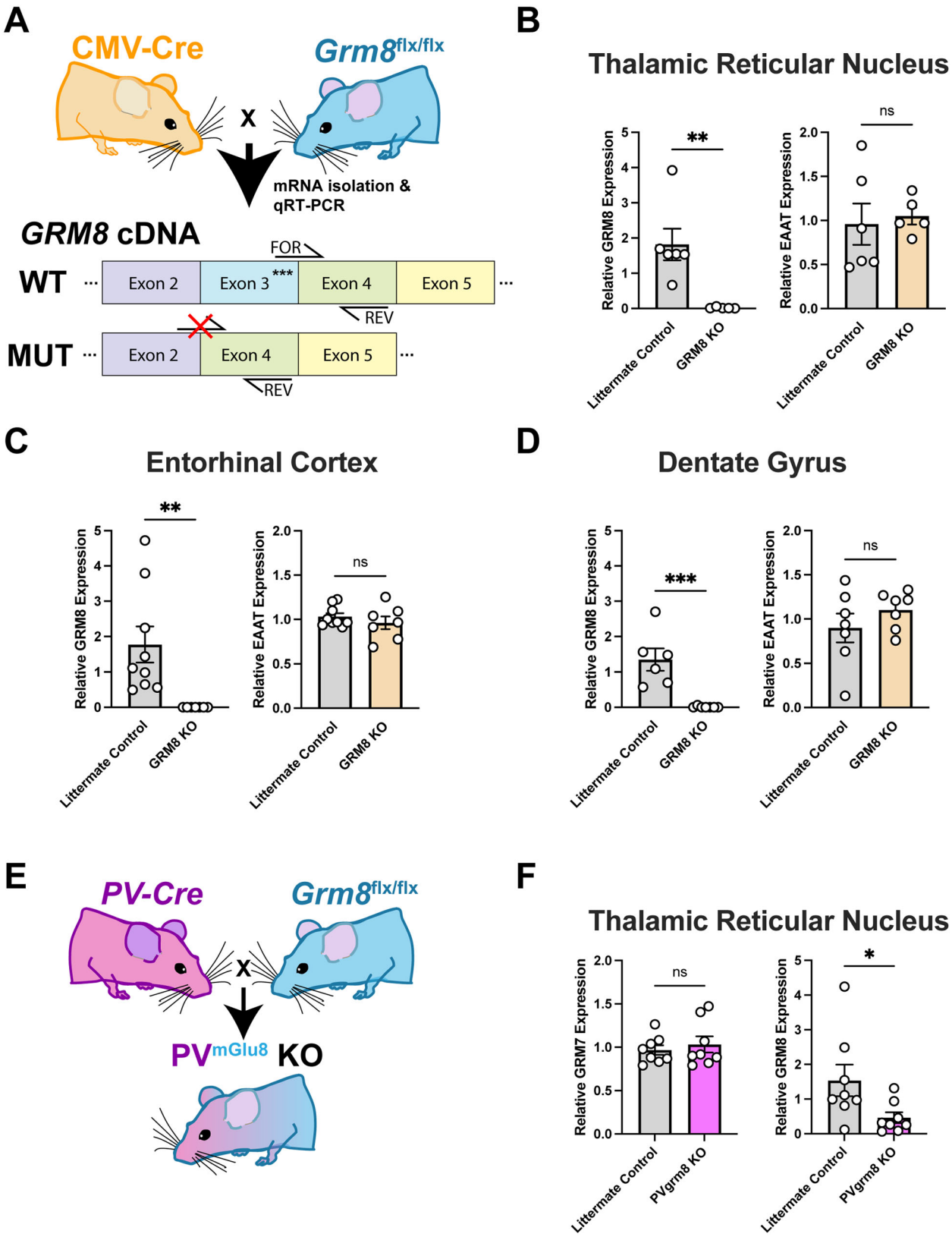

Figure 2. Validation of conditional *grm8* KO line via qRT-PCR. ***A***, Experimental schema depicting breeding cross and cDNA primer binding locations in WT and MUT animals. ***B–D***, Relative *grm8* and excitatory amino acid transporter 1 (EAAT) expression (compared with housekeeping gene *HPRT*) in the TRN, entorhinal cortex, and dentate gyrus of *grm8* KO mice and littermate controls. ***E***, Generation of PV-specific constitutive *grm8* KO mice. ***F***, Relative *grm7* and *grm8* expression in TRN tissue samples from PV^{grm8} KO and littermate control mice.

Finally, we calculated the excitatory:inhibitory neurotransmission ratios for PV^{grm8} KO and littermate control animals using three parameters: area, amplitude, and frequency. We observed no differences in E:I when using the area (total net charge) parameter (Fig. 3*D*; $t_{22} = 0.4778$, $p = 0.6375$, n.s.; control: 0.2833 ± 0.08 vs PV^{grm8} KO: 0.3525 ± 0.6146) or the $E:I_{amplitude}$

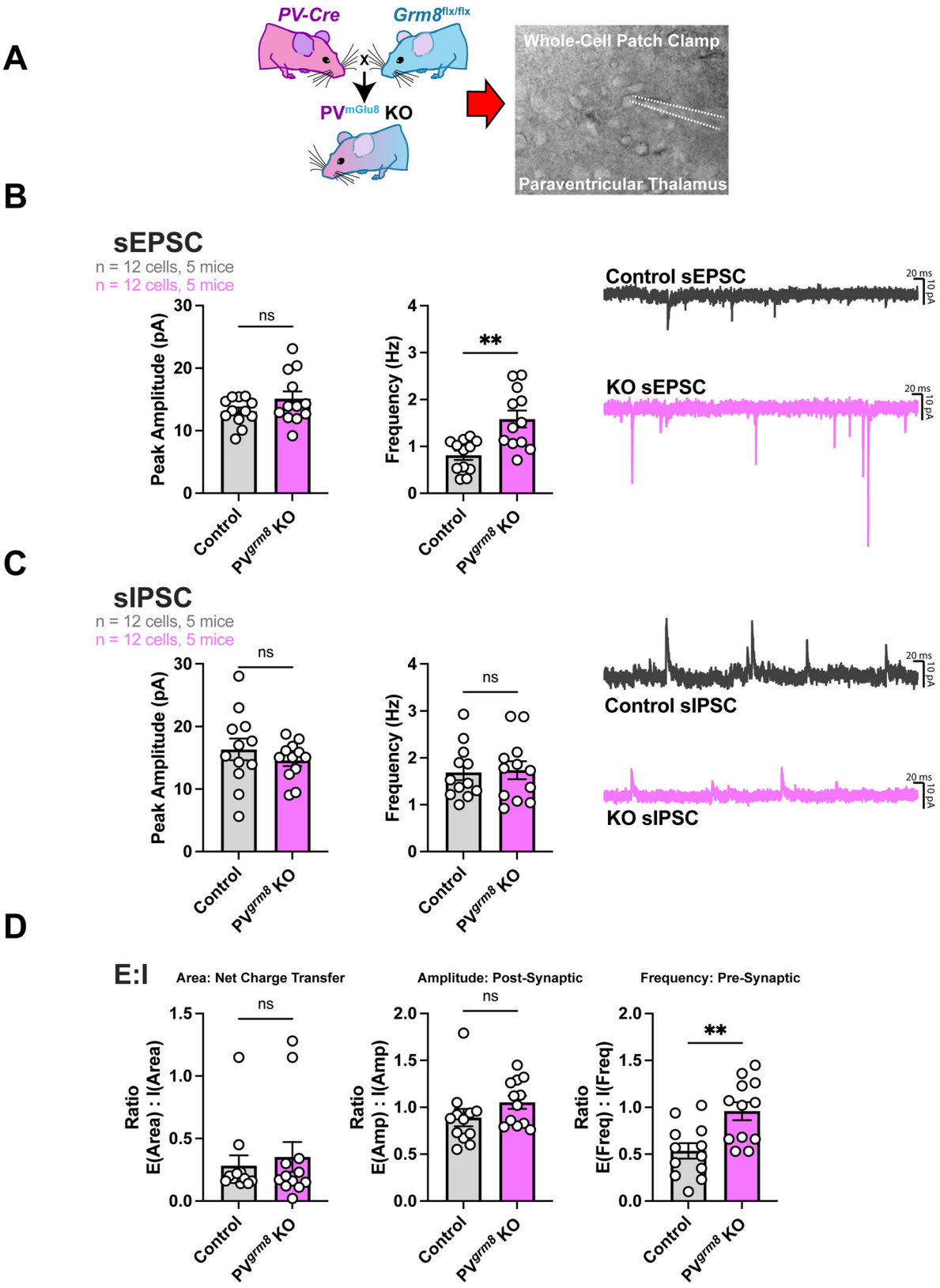

Figure 3. Altered neurotransmission onto PVT cells in PV^{grm8} KO mice. ***A***, Experimental design for whole-cell patch-clamp electrophysiology experiments in the paraventricular thalamus of PV^{grm8} KO mice. ***B***, Spontaneous excitatory neurotransmission frequency but not amplitude was increased in PV^{GRM8} KO mice. ***C***, Spontaneous inhibitory neurotransmission onto PVT cells was unaltered by PV^{grm8} KO. ***D***, E:I ratio determined by net charge transfer (E:I$_{area}$) and E:I$_{amplitude}$ were unchanged by PV^{grm8} KO, while E:I$_{frequency}$ was increased in PV^{GRM8} KO animals. Data were analyzed by Student's two-tailed, unpaired *t* test.

parameter ($t_{22} = 1.395$, $p = 0.1771$, n.s.; control: 0.89 ± 0.09 vs PV^{grm8} KO: 1.053 ± 0.07). We did observe increased E:I$_{frequency}$ ($t_{22} = 3.356$, $^{**}p = 0.0029$; control: 0.5350 ± 0.08 vs PV^{grm8} KO: 0.9583 ± 0.09). Together, these data imply that excitatory synaptic transmission onto thalamic cells is dysregulated in PV^{grm8} KO animals.

PV^{grm8} KO had no effect on locomotor habituation or anxiety phenotypes in repeated bouts of OFT

Early studies utilizing global *grm8* KO mice resulted in various anxiety and hyper- or hypolocomotive phenotypes (Gerlai et al., 2002; Linden et al., 2002; Robbins et al., 2007; Fendt et al., 2010; Lüffe et al., 2022), but did not allow insight into which *grm8*-expressing cell types and brain regions regulate these behaviors. We performed behavioral analyses with PV^{grm8} KO mice to determine if PV+ *grm8*+ cells regulate sensorimotor behaviors in nonconditioned measures of anxiety. PV^{grm8} KO animals first were observed in EZM and then were run through repeated bouts of OFT to determine the necessity of PV cell-specific *grm8* expression in regulating anxiety phenotypes along with thigmotaxis and locomotor habituation (Fig. 4*A*), as suggested by other studies (Gerlai et al., 2002; Lüffe et al., 2022).

Littermate control and PV^{grm8} KO mice were tested in the EZM for 5 min per trial. KO mice showed no differences in time spent in the open arms (Fig. 4*B*; Student's two-tailed *t* test, $t_{18} = 0.06928$, $p = 0.9455$, n.s.) or in entries into the open arms (Fig. 4*B*; Student's two-tailed *t* test, $t_{18} = 0.6595$, $p = 0.5179$, n.s.), suggesting no effect of KO on anxiety phenotypes. We observed no effects of PV^{grm8} KO on total distance traveled compared with littermate controls over 3 testing days [Fig. 4*B*; main effect of genotype on total distance: $F_{(1,18)} = 0.1070$, $p = 0.7473$, n.s., main effect of day on total distance: $F_{(1.840,\ 33.12)} = 10.39$, $^{***}p = 0.0004$, day × genotype interaction: $F_{(2,36)} = 1.825$, $p = 0.1757$, n.s.] nor was there a zone-dependent effect on locomotor activity [Fig. 4*B*, main effect of genotype on total center distance: $F_{(1,18)} = 0.06339$, $p = 0.8041$, n.s., main effect of day on total center distance: $F_{(1.685,\ 30.33)} = 19.15$, $p < 0.0001$, day × genotype interaction: $F_{(2,36)} = 2.565$, $p = 0.0909$, n.s.].

We next analyzed the habituation activity of PV^{grm8} KO mice and detected no differences in mutant activity levels over time compared with littermate controls, suggesting that there was no disruption of sensorimotor habituation [Fig. 4*C*; Day 1: main effect of genotype on day 1 habituation: $F_{(1,18)} = 0.1080$, $p = 0.7462$, n.s., main effect of day on Day 1 habituation: $F_{(5.019,\ 90.35)} = 44.42$, $^{****}p < 0.0001$, day × genotype interaction: $F_{(11,198)} = 1.122$, $p = 0.3457$, n.s.; Day 2: main effect of genotype on Day 2 habituation: $F_{(1,18)} = 0.5144$, $p = 0.4824$, n.s., main effect of day on Day 2 habituation: $F_{(4.410,\ 79.37)} = 24.35$, $^{****}p < 0.0001$, day × genotype interaction: $F_{(11,198)} = 1.336$, $p = 0.2070$, n.s.; Day 3: main effect of genotype on Day 2 habituation: $F_{(1,18)} = 1.257$, $p = 0.2770$, n.s., main effect of day on Day 2 habituation: $F_{(5.841,\ 105.1)} = 14.76$, $^{****}p < 0.0001$, day × genotype interaction: $F_{(11,198)} = 1.081$, $p = 0.3786$, n.s.].

Furthermore, cumulative distance traveled over time in the center zone was unaffected by PV^{grm8} KO [Fig. 4*D*; main effect of genotype on Day 1 cumulative center zone distance: $F_{(1,17)} = 0.2600$, $p = 0.6167$, n.s., main effect of day on Day 1 cumulative center zone distance: $F_{(1.148,\ 19.52)} = 52.46$, $^{****}p < 0.0001$, genotype × day interaction: $F_{(11,187)} = 0.04351$, $p > 0.9999$, n.s.; main effect of genotype on Day 2 cumulative center zone distance: $F_{(1,17)} = 2.045$, $p = 0.1709$, n.s., main effect of day on Day 2 cumulative center zone distance: $F_{(1.112,\ 18.91)} = 19.49$, $^{***}p = 0.0002$, genotype × day interaction: $F_{(11,187)} = 0.9975$, $p = 0.4503$, n.s.; main effect of genotype on Day 3 cumulative center zone distance: $F_{(1,17)} = 0.6846$, $p = 0.4195$, n.s., main effect of day on Day 3 cumulative center zone distance: $F_{(1.051,\ 17.87)} = 13.42$, $^{**}p = 0.0016$, genotype × day interaction: $F_{(11,187)} = 0.8531$, $p = 0.5873$, n.s.]. Finally, we determined that there were no differences between KO and littermate controls in the amount of time spent in the center zone of the testing arena [Fig. 4*E*; main effect of genotype on normalized center time: $F_{(1,18)} = 0.6466$, $p = 0.4318$, n.s., main effect of day on normalized center time: $F_{(1.904,\ 34.27)} = 28.65$, $^{****}p < 0.0001$, genotype × day interaction: $F_{(2,36)} = 3.507$, $^{*}p = 0.0406$; main effect of genotype on normalized peripheral time: $F_{(1,18)} = 0.6459$, $p = 0.4321$, n.s., main effect of day on normalized peripheral time: $F_{(1.904,\ 34.27)} = 28.62$, $^{****}p < 0.0001$, genotype × day interaction: $F_{(2,36)} = 3.503$, $^{*}p = 0.0407$]. Together, these data suggest that mGlu8 signaling on PV cells is not necessary for expression of OFT phenotypes (Gerlai et al., 2002; Robbins et al., 2007).

PV^{grm8} KO produced deficits in acoustic startle and PPI

Numerous reports have studied TRN (Wells et al., 2016; You et al., 2021) and *grm8* (Fendt et al., 2010; Hikichi et al., 2010) signaling in the regulation of acoustic startle and PPI, a well-established assay used in preclinical and clinical models to identify deficits in sensorimotor gating associated with various neuropsychiatric disorders. We utilized our PV^{grm8} KO model to determine whether *grm8* signaling on PV cells regulates sensorimotor gating (Fig. 5*A*).

Subjects were tested for basal startle activity via a startle curve where tones without prepulses were played (Fig. 5*B*). There was no effect of genotype on startle magnitude and a significant effect of tone intensity but no overall genotype × tone intensity interaction [Fig. 5*B*; two-way RM-ANOVA; effect of genotype: $F_{(1,8)} = 0.1543$, $p = 0.7047$, n.s.; effect of tone intensity: $F_{(1.22,\ 8.979)} = 31.59$, $^{***}p = 0.0003$, genotype × tone intensity: $F_{(5,40)} = 1.403$, $p = 0.2439$, n.s.]. We observed main effects of genotype and of tone intensity on the baseline startle response to 120 dB [Fig. 5*C*; two-way RM-ANOVA; effect of genotype: $F_{(1,7)} = 6.474$, $^{*}p = 0.0384$, effect of tone intensity: $F_{(1,7)} = 225.8$, $^{***}p < 0.0001$, genotype × tone intensity: $F_{(1,7)} = 7.598$, $^{*}p = 0.0282$]. To test the sensorimotor gating functionality of our subjects, we then tested for altered startle magnitude by randomly pairing 70, 76, 82, and 88 dB prepulse tones with our 0 and 120 dB test tones. We found that prepulse + tone presentation decreased the startle magnitude of PV^{grm8} KO mice compared with littermate controls [Fig. 5*D*; two-way RM-ANOVA; effect of genotype: $F_{(1,7)} = 6.568$, $^{*}p = 0.0374$, effect of tone intensity: $F_{(1.852,\ 12.96)} = 3.429$, n.s. $p = 0.0666$; genotype × startle intensity: $F_{(3,21)} = 0.8242$, n.s. $p = 0.4952$] regardless of prepulse intensity. Conversely, we did not observe statistically significant changes in percent inhibition of startle responses in our mutant model [Fig. 5*E*; two-way RM-ANOVA; effect of genotype: $F_{(1,7)} = 3.175$, n.s. $p = 0.1180$; effect of startle intensity: $F_{(1.968,\ 13.78)} = 3.870$, $^{*}p = 0.0469$; genotype × startle intensity: $F_{(3,21)} = 0.9931$, n.s. $p = 0.4153$].

TRN-specific *grm8* KD disrupts sensorimotor activity and produces hyperlocomotive phenotypes

As *grm8* is expressed throughout the TC system, we sought to identify region-specific gene functionality. We hypothesized that deletion of *grm8* in discrete TC nuclei could reveal region-specific regulation of OFT behavior. To test this hypothesis, based on other reports implicating the TRN in thigmotaxis (Wells et al., 2016; El Boukhari et al., 2019), we utilized our

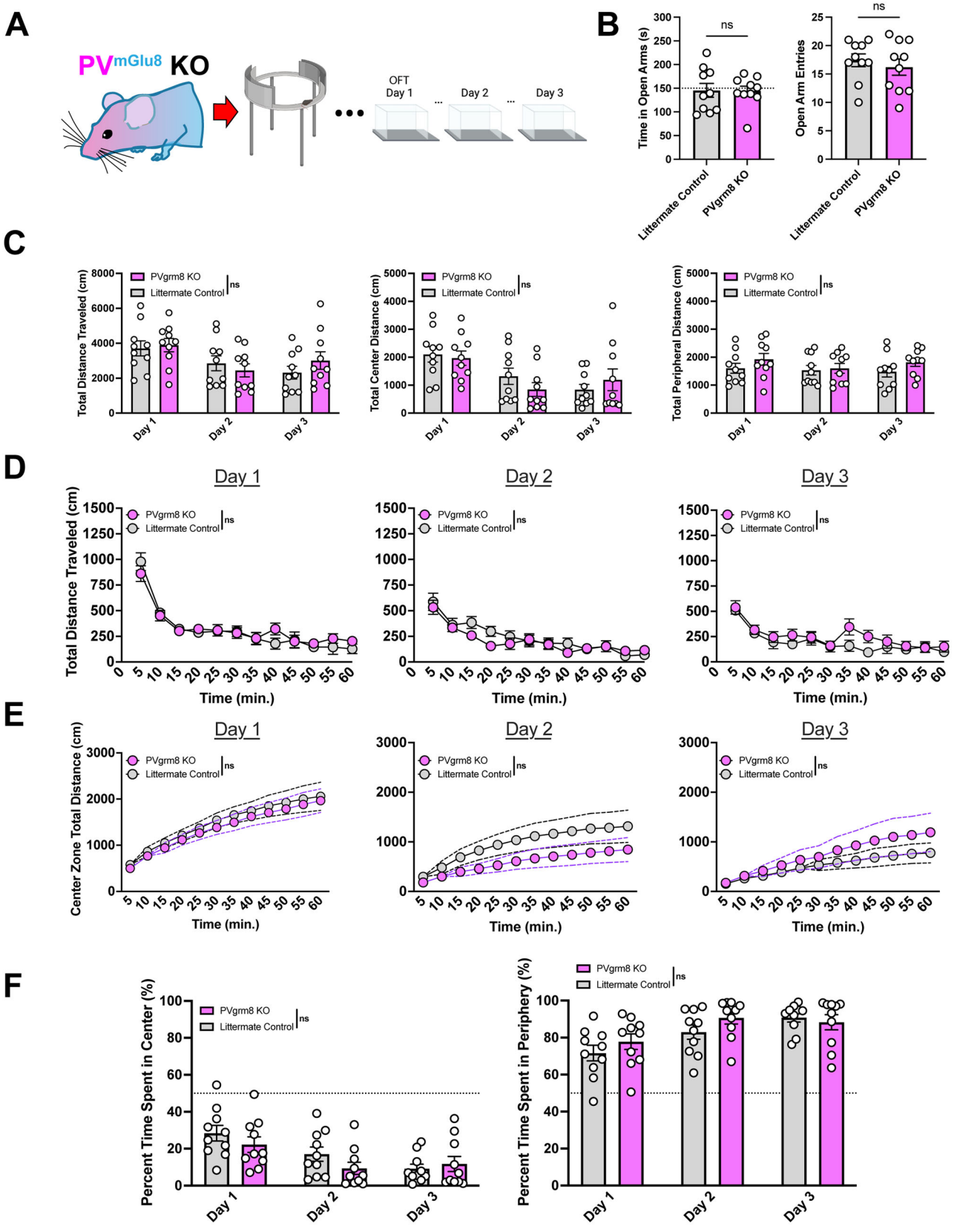

Figure 4. PV^{grm8} KO did not affect sensorimotor habituation in EZM or repeated open field sessions. ***A***, Experimental design. ***B***, No differences in time spent in open arms or entries into open arms were noted between experimental and control groups. ***C***, There were no statistically significant main effects of genotype on the total distance traveled, the distance traveled in the center zone, or the distance traveled in the peripheral zone. ***D***, KO did not affect locomotor activity over time compared with littermate controls. ***E***, Cumulative center zone distances were unaffected by PV^{grm8} KO. ***F***, No effects of genotype were observed in normalized time spent in the center or peripheral zones, reflected as a percentage of the total test duration. All statistical tests are run as two-way RM-ANOVA including with noncorrected Fisher's LSD post hoc test.

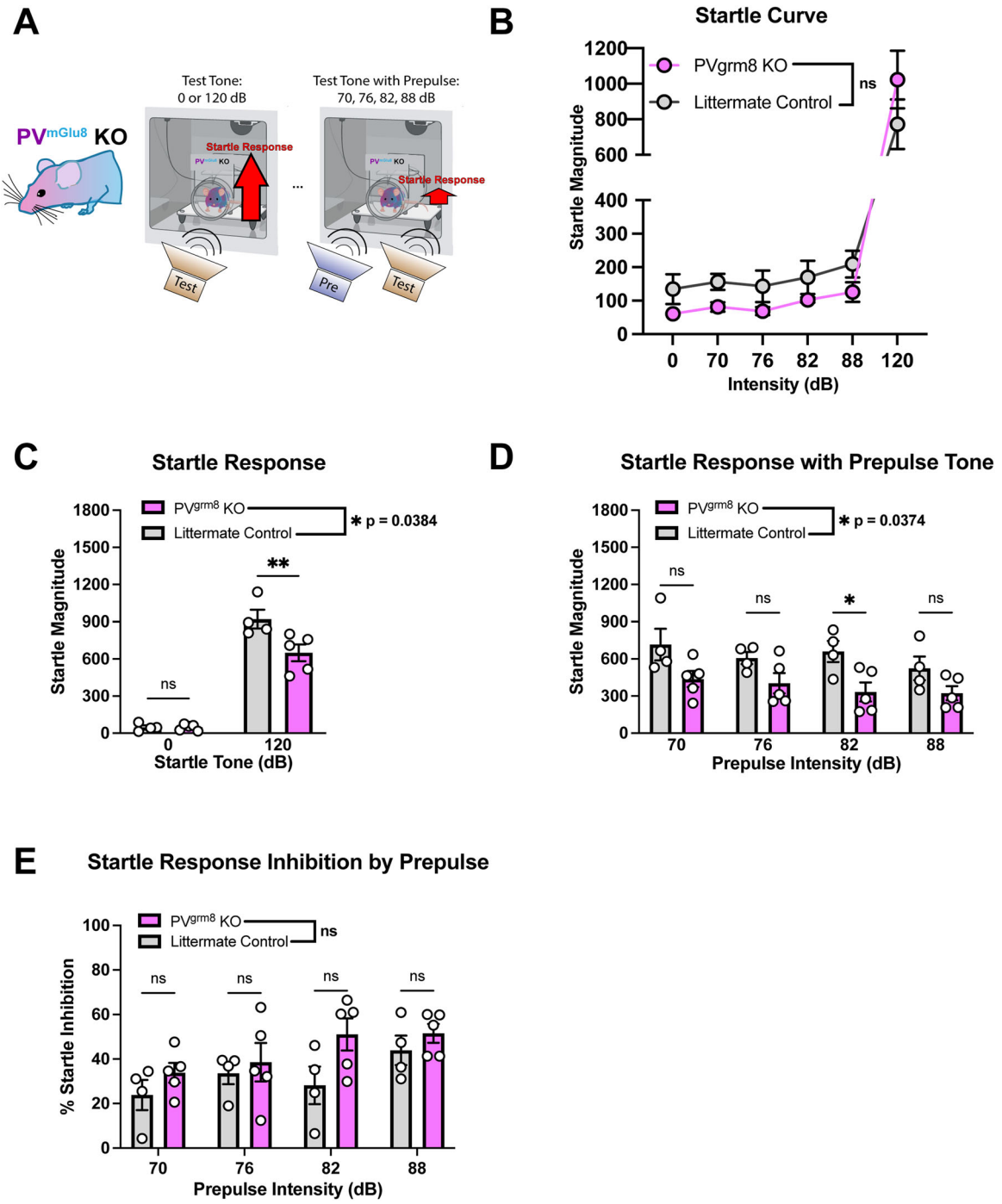

Figure 5. ***A***, Schema depicting acoustic startle and PPI paradigms. ***B***, Differences in basal responses to tone intensities (no prepulses) were not statistically significant between groups. ***C***, Baseline acoustic startle magnitudes were decreased in PV^{grm8} KO but not littermate controls. ***D***, Startle magnitudes were decreased in PV^{grm8} KO by presentation of prepulse tone regardless of tone intensity. ***E***, PPI trended high in PV^{grm8} KO animals but did not reach statistical significance.

floxed *grm8* model to KD *grm8* expression specifically within the TRN (TRN^{grm8} KD; Fig. 6*A*).

We sought to determine the effects of KD on locomotion and first analyzed zone-specific total locomotor activity in KD versus control animals over 3 testing days. There was a main effect of KD and of time on total distance traveled regardless of zone [Fig. 6*B*; two-way RM-ANOVA effect of KD on total distance; effect of KD: $F_{(1,12)} = 7.941$, $^{*}p = 0.0155$; effect of time: $F_{(1.226,\ 14.72)} = 9.672$]. Interestingly, the hyperlocomotion phenotype observed in the experimental group was specific to the center zone of the testing apparatus [Fig. 5*B*, two-way RM-ANOVA effect of KD on center total distance; effect of KD: $F_{(1,12)} = 9.222$, $^{*}p = 0.0103$; effect of time: $F_{(1.154,\ 13.85)} = 10.07$, $^{**}p = 0.0054$]. There was no statistically significant difference between KD and control groups in total distance traveled in the surround zone [Fig. 5*B*; two-way RM-ANOVA effect of KD on surround distance; effect of KD: $F_{(1,12)} = 2.798$, $p = 0.1202$, n.s.; effect of time: $F_{(1.812,\ 21.75)} = 2.147$, $p = 0.1445$, n.s.].

We next analyzed the raw habituation activity of the animals to the open field zones over time. The experimental KD group

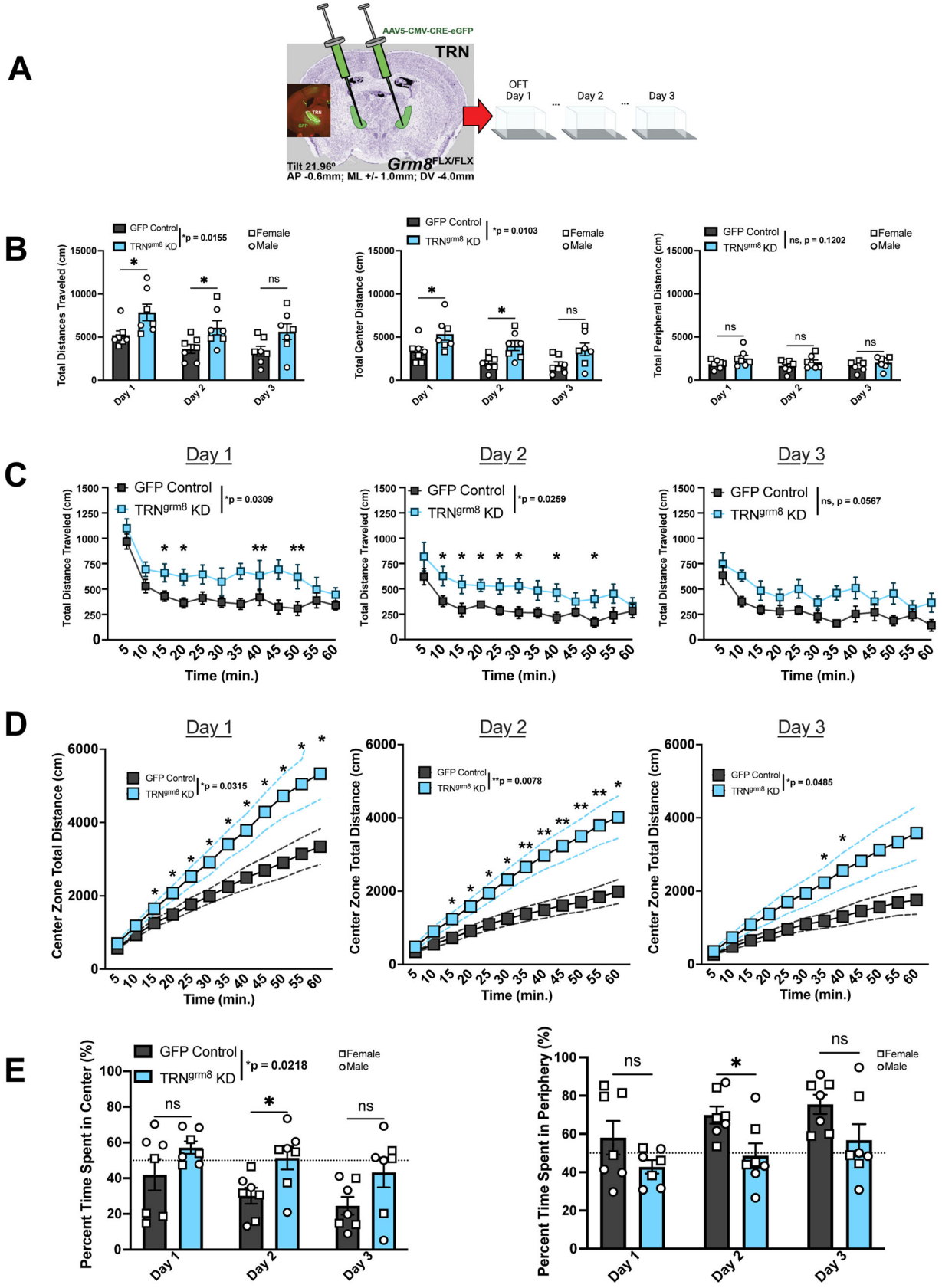

Figure 6. TRN^{grm8} ablation alters sensorimotor habituation activity in repeated OFT. ***A***, Experimental design and stereotax coordinates targeting rostroventral TRN. ***B***, There was a statistically significant main effect of KD on the total distance traveled and the total center distance traveled in the open field but not in the peripheral zone. ***C***, TRN^{grm8} KD mice exhibited increased basal activity levels over 3 testing days. ***D***, Cumulative center zone-specific activity levels were increased in experimental animals compared with control over 3 testing days. ***E***, KD-dependent increase in time spent in the center zone and decreased time in the peripheral zone. All statistical tests are run as two-way RM-ANOVA including with noncorrected Fisher's LSD post hoc test.

exhibited disrupted habituation levels on each testing day, indicated by consistently increased basal activity levels [Fig. 6*C*; effect of KD Day 1: $F_{(1,12)} = 5.980$, $p = 0.0309$; effect of KD Day 2: $F_{(1,12)} = 6.461$, $p = 0.0259$; effect of KD Day 3: $F_{(1,12)} = 4.446$, $p = 0.0567$], whereas the control animals decreased their locomotor behaviors with each testing day. We found that TRN^{grm8} KD animals traveled greater cumulative total distances over time specifically in the center zone of the open field apparatus, an effect that appeared at ~15 min into testing [Fig. 6*D*; effect of KD on cumulative center activity; Day 1 cumulative sum: $F_{(1,12)} = 5.922$, $^{*}p = 0.0315$; Day 2 cumulative sum: $F_{(1,12)} = 10.16$, $^{**}p = 0.0078$; Day 3 cumulative sum: $F_{(1,12)} = 4.823$, $^{*}p = 0.0485$]. In addition to locomotion, TRN^{grm8} KD animals also spent ~50% or more of their time in the center zone of the open field when normalized to total testing time [Fig. 6*E*; effect of KD on normalized center time; effect of KD: $F_{(1,12)} = 6.942$ $^{*}p = 0.0218$; effect of time: $F_{(1.474,\ 17.69)} = 4.870$ $^{*}p = 0.0290$]. Nonsurprisingly, *grm8* KD mice consistently spent less time in the surround zone compared with control animals.

Together, the combined behavioral profiles of PV^{grm8} KO and TRN^{grm8} KD animals suggests that *grm8* plays a role in regulating sensorimotor activity and anxiety phenotypes in the open field assay likely through changes in neurotransmission throughout the TC system.

Discussion

In the present study, we demonstrated that the mGlu8 receptor-encoding gene *grm8* regulates neurotransmission onto dorsal thalamic relay cells and the behavioral outputs of the TC network. Low-density expression of *grm8*+ cells were detected in the medial and midline thalamic nuclei, TRN, and nearly all layers of the somatosensory cortex, suggesting that in these regions, only a small fraction of all cells are *grm8*+. Conversely, strong coexpression of *grm8* with PV was observed in the TRN and deeper cortical layers known to project to the dorsal thalamus and TRN. Through the use of a floxed *grm8* mouse, we show that PV-specific constitutive *grm8* KO (PV^{grm8} KO) increased the frequency of spontaneous excitatory but not inhibitory transmission onto thalamic relay neurons located within the PVT, a critical nucleus for expression of a variety of behaviors. PV^{grm8} KO did not affect locomotor habituation and anxiety-like phenotypes in EZM and open field assays but did produce KO-dependent effects on acoustic startle magnitude, suggesting involvement of PV+ *grm8*+ cells not in locomotion but in sensorimotor gating. We then showed that *grm8*+ TRN cells regulated OFT habituation, locomotor, and anxiety phenotypes via viral-mediated conditional KD. Altogether, we found that *grm8*+ cells in the TC–CT system regulate spontaneous excitatory synaptic transmission onto thalamic relay neurons and facilitate sensorimotor gating of extraneous stimuli in open field and acoustic startle assays. The behavioral phenotypic differences observed in the two different KD approaches could be related to differences in the timing of the deletion relative to development and/or the nonoverlapping cell populations targeted in the two approaches beyond TRN PV cells.

Group III mGlu receptors are involved in the expression of anxiety- and stress-related behavioral phenotypes (Pałucha et al., 2004; Goddyn et al., 2015; for review, see Dogra and Conn, 2021). In classical, nonconditioned measures of anxiety, constitutive *grm8* KO mice showed altered locomotor activity in open field [Duvoisin et al., 2005; Lüffe et al., 2022; both decreased (Duvoisin et al., 2005) and increased (Gerlai et al., 2002)], increased anxiety phenotypes in the elevated plus maze (Linden et al., 2002; Duvoisin et al., 2005), as and deficits in contextual fear, object recognition, and PPI (Fendt et al., 2010). Findings in zebrafish suggest that deletion of both *grm8*$_A$ and *grm8*$_B$ isoforms disrupted normal thigmotaxis behavior, further suggesting a role of *grm8* in guiding behavioral responses relative to an organism's environment (Lüffe et al., 2022). Notably, Linden et al. (2003a) reported increased levels of the neuronal activity marker cFos in medial thalamus relay neurons following EPM exposure in *grm8* KO mice, further supporting the hypothesis that *grm8* regulates behavioral responses to aversive environments. The present study adds to these findings by implicating *grm8* function within the TC–TRN–CT system in aspects of sensorimotor gating and locomotion, likely by regulating neurotransmission within the dorsal thalamus.

This study is in line with other published reports demonstrating mGlu8-dependent anxiety and locomotor behaviors (Duvoisin et al., 2005), as well as those implicating *grm8* in the regulation of acoustic startle and PPI (Robbins et al., 2007; Fendt et al., 2010). Through our conditional deletion approaches, we suggest that TRN^{grm8} KD (facilitated by a viral-mediated strategy), but not constitutive PV^{grm8} KO, disrupted normal sensorimotor habituation and activity in repeated bouts of OFT. We further show that deficits in acoustic startle and PPI are regulated by *grm8* expressed specifically on PV neurons. Together, our findings suggest mGlu8 is a critical mediator of sensorimotor behaviors, potentially through the regulation of the cortical output to the thalamus. Furthermore, our findings underscore existing preclinical and human genetics literature implicating the TC–TRN–CT system and *grm8* in the pathogenesis of a variety of neuropsychiatric disorders characterized by negative affect (Terracciano et al., 2010) and externalizing behaviors (Bauer and Covault, 2020; A. C. H. Chen et al., 2009; Gast et al., 2013; Kostrzewa et al., 2015; Long et al., 2015). In addition, our PV-specific deletions agree with and highlight published reports exploring functionality of PV neurons in various neuropsychiatric disorders (Steullet et al., 2018; Cabungcal et al., 2019; Perlman et al., 2021; Radovanovic et al., 2021).

Mechanistically, little is understood about the role of mGlu8 signaling within the TC system. Here, we showed that mGlu8 receptors expressed by PV neurons regulated spontaneous excitatory neurotransmission onto thalamic neurons. A surprising result of the present study was that inhibitory neurotransmission onto the same cells was unaffected by PV^{grm8} KO, given the high degree of *grm8* and PV co-expression in the GABAergic TRN. Despite the lack of inhibitory regulation in this report, other reports demonstrated a role of mGlu8 in regulating glutamatergic and GABAergic transmission in other brain regions (Marabese et al., 2005, 2007; Palazzo et al., 2011). We hypothesize that the observed increase in excitatory drive onto thalamic relay neurons in PV^{grm8} KO mice is a result of cortical PV interneuron microcircuit dysfunction, whereby removal of mGlu8 on cortical PV cells facilitates increased pyramidal cell drive onto TC cells. Together, these data imply that synaptic transmission onto thalamic cells is dysregulated in PV^{grm8} KO animals likely through disrupted CT signaling. Future studies utilizing electrophysiological, behavioral, and cortical EEG techniques will determine roles of mGlu8 in regulating TRN- and cortical-specific PV^{grm8+} cell function and how these unique neural systems guide behavior in murine models of externalizing disorders.

The mouse models used in these studies provide novel insight into the neurobiology of mGlu8. However, there are limitations associated with both the constitutive parvalbumin-specific KO and TRN-specific viral-mediated KD of *grm8* that affect

interpretation of the presented data. The presented findings in PV^{grm8} KO mice cannot be attributed solely to the TRN and alterations in TRN signaling. It is possible that the increased excitatory synaptic transmission was due to alterations in cortical interneuron and pyramidal cell signaling. The lack of effect on inhibitory synaptic transmission in PV^{grm8} KO mice is indeed suggestive of synaptic alterations occurring outside of the TRN. Conversely, the conditional TRN^{grm8} KD effects on habituation behavior do not differentiate between the numerous cell types in the TRN (Y. Li et al., 2020). Despite these limitations, the two mouse models presented here advance our understanding of mGlu8 function within the TC circuitry, adding to growing bodies of literature on the roles of *grm8*, PV expression neurons, and the TRN in neuropsychiatric and neurological disorders (Krol et al., 2018; Steullet et al., 2018; Bauer and Covault, 2020; Nahar et al., 2021; Lüffe et al., 2022).

The ability of mGlu receptors to form obligate dimers and the dimerizing potential of Group II and Group III mGlu receptors were previously reported in vitro (Doumazane et al., 2011). More recent findings (Lin et al., 2022) have implicated pharmacologically distinct mGlu7/8 receptor dimers in regulating the activity of the SC-CA1 hippocampal synapse in vivo. With regard to the lack of mGlu8 regulation of inhibitory transmission, it is possible that PV-dense TRN cells synapsing onto TC cells could compensate for constitutive *grm8* deletion over the course of development by substituting another mGlu receptor in mGlu8's place. Of the Group III mGlu receptors, the expression of *grm7* and *grm8* in the TRN is high, while *grm4* mRNA was not detected (in situ data not shown), and *grm6* is exclusively expressed in the retina, leaving mGlu2 and mGlu3 as the other remaining dimerizing partners in the TRN. The availability of novel and specific dimer-preferring small molecules, as shown by Lin et al. (2022), will greatly facilitate experiments exploring the functionality of mGlu heterodimers.

Altogether, the present study adds to a growing body of literature that has implicated mGlu8, the TC system, and TRN in various neurophysiological roles and sensorimotor phenotypes. Furthermore, by highlighting the use of novel genetic technologies and deletion strategies, we lay groundwork that will serve as a basis to study mGlu8 regulation of the TC system via the TRN in more depth.

Conclusion

Group III mGlu receptors are critical modulators of neurotransmission involved in sensory perception, and their dysfunction is implicated in numerous psychiatric and neurologic disorders. mGlu8 regulation of inhibitory TRN terminals maintains normal electrophysiological properties of neurons within the dorsal thalamus, allowing for proper information flow from the thalamus to the cortex. Expanding our understanding of how the brain regulates sensorimotor activity and attention may represent novel loci for therapeutic drug development, potentially for the treatment of CNS disorders such as anxiety and substance abuse. The proven efficacy of therapeutically targeting mGlu receptors highlights the importance of this study.

References

Bauer LO, Covault JM (2020) GRM8 genotype is associated with externalizing disorders and greater inter-trial variability in brain activation during a response inhibition task. Clin Neurophysiol 131:1180–1186.

Bradley A, et al. (2012) The mammalian gene function resource: The International Knockout Mouse Consortium. Mamm Genome 23:580–586.

Cabungcal JH, Steullet P, Kraftsik R, Cuenod M, Do KQ (2019) A developmental redox dysregulation leads to spatio-temporal deficit of parvalbumin neuron circuitry in a schizophrenia mouse model. Schizophr Res 213:96–106.

Carroll BJ, Sampathkumar V, Kasthuri N, Sherman SM (2022) Layer 5 of cortex innervates the thalamic reticular nucleus in mice. Proc Natl Acad Sci U S A 119:e2205209119.

Chen ACH, et al. (2009) Association of single nucleotide polymorphisms in a glutamate receptor gene (GRM8) with theta power of event-related oscillations and alcohol dependence. Am J Med Genet B Neuropsychiatr Genet 150:359–368.

Chen M, Bi LL (2019) Optogenetic long-term depression induction in the PVT-CeL circuitry mediates decreased fear memory. Mol Neurobiol 56:4855.

Dobi A, Sartori SB, Busti D, Van der Putten H, Singewald N, Shigemoto R, Ferraguti F (2013) Neural substrates for the distinct effects of presynaptic group III metabotropic glutamate receptors on extinction of contextual fear conditioning in mice. Neuropharmacology 66:274–289.

Dogra S, Conn PJ (2021) Targeting metabotropic glutamate receptors for the treatment of depression and other stress-related disorders. Neuropharmacology 196:1.

Doumazane E, Scholler P, Zwier JM, Trinquet E, Rondard P, Pin J (2011) A new approach to analyze cell surface protein complexes reveals specific heterodimeric metabotropic glutamate receptors. FASEB J 25:66–77.

Duvoisin RM, Zhang C, Pfankuch TF, O'Connor H, Gayet-Primo J, Quraishi S, Raber J (2005) Increased measures of anxiety and weight gain in mice lacking the group III metabotropic glutamate receptor mGluR8. Eur J Neurosci 22:425–436.

Duvoisin RM, Zhang C, Ramonell K (1995) A novel metabotropic glutamate receptor expressed in the retina and olfactory bulb. J Neurosci 15:3075–3083.

El Boukhari H, Ouhaz Z, Ba-M'hamed S, Bennis M (2019) Early lesion of the reticular thalamic nucleus disrupts the structure and function of the mediodorsal thalamus and prefrontal cortex. Dev Neurobiol 79:913–933.

El Khoueiry C, Cabungcal JH, Rovó Z, Fournier M, Do KQ, Steullet P (2022) Developmental oxidative stress leads to T-type Ca2+ channel hypofunction in thalamic reticular nucleus of mouse models pertinent to schizophrenia. Mol Psychiatry 27:2042.

Fendt M, Bürki H, Imobersteg S, Van Der Putten H, McAllister K, Leslie JC, Shaw D, Hölscher C (2010) The effect of mGlu8 deficiency in animal models of psychiatric diseases. Genes Brain Behav 9:33–44.

Ferraguti F (2018) Metabotropic glutamate receptors as targets for novel anxiolytics. Curr Opin Pharmacol 38:37–42.

Ferrarelli F, Tononi G (2011) The thalamic reticular nucleus and schizophrenia. Schizophr Bull 37:306–315.

Fetterly TL, Basu A, Nabit BP, Awad E, Williford KM, Centanni SW, Matthews RT, Silberman Y, Winder DG (2019) α2A-adrenergic receptor activation decreases parabrachial nucleus excitatory drive onto BNST CRF neurons and reduces their activity in vivo. J Neurosci 39:472.

Gast MT, et al. (2013) The role of rs2237781 within GRM8 in eating behavior. Brain Behav 3:495–502.

Gerardo CM, Manuel MMV (2020) The thalamic reticular nucleus: a common nucleus of neuropsychiatric diseases and deep brain stimulation. J Clin Neurosci 73:1–7.

Gerlai R, Adams B, Fitch T, Chaney S, Baez M (2002) Performance deficits of mGluR8 knockout mice in learning tasks: the effects of null mutation and the background genotype. Neuropharmacology 43:235–249.

Goddyn H, Callaerts-Vegh Z, D'Hooge R (2015) Functional dissociation of group III metabotropic glutamate receptors revealed by direct comparison between the behavioral profiles of knockout mouse lines. Int J Neuropsychopharmacol 18:1.

Gosnell HB, Silberman Y, Grueter BA, Duvoisin RM, Raber J, Winder DG (2011) Mglur8 modulates excitatory transmission in the bed nucleus of the stria terminalis in a stress-dependent manner. Neuropsychopharmacology 36:1599–1607.

Green L, Green L (2022) Characteristics and function of PVT synaptic inputs to NAc cell populations following opioid use.

Harris NA, et al. (2018) Dorsal BNST α2A-adrenergic receptors produce HCN-dependent excitatory actions that initiate anxiogenic behaviors. J Neurosci 38:8922.

Hikichi H, Nishino M, Fukushima M, Satow A, Maehara S, Kawamoto H, Ohta H (2010) Pharmacological effects of metabotropic glutamate receptor ligands on prepulse inhibition in DBA/2J mice. Eur J Pharmacol 639:99–105.

James MH, Dayas CV (2013) What about me…? The PVT: a role for the paraventricular thalamus (PVT) in drug-seeking behaviour. Front Behav Neurosci 7:18.

John YJ, Zikopoulos B, Bullock D, Barbas H (2016) The emotional gatekeeper: a computational model of attentional selection and suppression through the pathway from the amygdala to the inhibitory thalamic reticular nucleus. PLoS Comput Biol 12:e1004722.

Kawaguchi Y, Kubota Y (1997) GABAergic cell subtypes and their synaptic connections in rat frontal cortex. Cereb Cortex 7:476–486.

Kostrzewa E, Brandys MK, van Lith HA, Kas MJH (2015) A candidate syntenic genetic locus is associated with voluntary exercise levels in mice and humans. Behav Brain Res 276:8–16.

Krol A, Wimmer RD, Halassa MM, Feng G (2018) Thalamic reticular dysfunction as a circuit endophenotype in neurodevelopmental disorders. Neuron 98:282–295.

Lam YW, Sherman SM (2007) Different topography of the reticulothalmic inputs to first- and higher-order somatosensory thalamic relays revealed using photostimulation. J Neurophysiol 98:2903–2909.

Lee JH, Latchoumane CFV, Park J, Kim J, Jeong J, Lee KH, Shin HS (2019) The rostroventral part of the thalamic reticular nucleus modulates fear extinction. Nat Commun 10:1.

Li Y, et al. (2020) Distinct subnetworks of the thalamic reticular nucleus. Nature 583:819–824.

Li S, Kirouac GJ (2008) Projections from the paraventricular nucleus of the thalamus to the forebrain, with special emphasis on the extended amygdala. J Comp Neurol 506:263.

Li SH, Li S, Kirouac GJ (2024) Analysis of monosynaptic inputs to thalamic paraventricular nucleus neurons innervating the shell of the nucleus accumbens and central extended amygdala. Neuroscience 537:151–164.

Lin X, et al. (2022) Differential activity of mGlu7 allosteric modulators provides evidence for mGlu7/8 heterodimers at hippocampal Schaffer collateral-CA1 synapses. J Biol Chem 298:102458.

Linden A-M, Baez M, Bergeron M, Schoepp DD (2003a) Increased c-Fos expression in the centromedial nucleus of the thalamus in metabotropic glutamate 8 receptor knockout mice following the elevated plus maze test. Neuroscience 121:167–178.

Linden A-M, Bergeron M, Baez M, Schoepp DD (2003b) Systemic administration of the potent mGlu8 receptor agonist (S)-3,4-DCPG induces c-Fos in stress-related brain regions in wild-type, but not mGlu8 receptor knockout mice. Neuropharmacology 45:473–483.

Linden A-M, Johnson BG, Peters SC, Shannon HE, Tian M, Wang Y, Yu JL, Koster A, Baez M, Schoepp DD (2002) Increased anxiety-related behavior in mice deficient for metabotropic glutamate 8 (mGlu8) receptor. Neuropharmacology 43:251–259.

Long EC, Aliev F, Wang J-C, Edenberg HJ, Nurnberger JJ, Hesselbrock V, Porjesz B, Dick DM (2015) Further analyses of genetic association between GRM8 and alcohol dependence symptoms among young adults. J Stud Alcohol Drugs 76:414–418.

Lüffe TM, Bauer M, Gioga Z, Özbay D, Romanos M, Lillesaar C, Drepper C (2022) Loss-of-function models of the metabotropic glutamate receptor genes Grm8a and Grm8b display distinct behavioral phenotypes in zebrafish larvae (Danio rerio). Front Mol Neurosci 15:901309.

Marabese I, et al. (2007) Periaqueductal gray metabotropic glutamate receptor subtype 7 and 8 mediate opposite effects on amino acid release, rostral ventromedial medulla cell activities, and thermal nociception. J Neurophysiol 98:43–53.

Marabese I, de Novellis V, Palazzo E, Mariani L, Siniscalco D, Rodella L, Rossi F, Maione S (2005) Differential roles of mGlu8 receptors in the regulation of glutamate and gamma-aminobutyric acid release at periaqueductal grey level. Neuropharmacology 49:157–166.

Mease RA, Gonzalez AJ (2021) Corticothalamic pathways from layer 5: emerging roles in computation and pathology. Front Neural Circuits 15:730211.

Mercier MS, Lodge D, Fang G, Nicolas CS, Collett VJ, Jane DE, Collingridge GL, Bortolotto ZA (2013) Characterisation of an mGlu8 receptor-selective agonist and antagonist in the lateral and medial perforant path inputs to the dentate gyrus. Neuropharmacology 67:294–303.

Nahar L, Delacroix BM, Nam HW (2021) The role of parvalbumin interneurons in neurotransmitter balance and neurological disease. Front Psychiatry 12: 679960.

Niswender CM, Conn PJ (2010) Metabotropic glutamate receptors: physiology, pharmacology, and disease. Annu Rev Pharmacol Toxicol 50:295.

Palazzo E, Marabese I, Soukupova M, Luongo L, Boccella S, Giordano C, de Novellis V, Rossi F, Maione S (2011) Metabotropic glutamate receptor subtype 8 in the amygdala modulates thermal threshold, neurotransmitter release, and rostral ventromedial medulla cell activity in inflammatory pain. J Neurosci 31:4687–4697.

Pałucha A, Tatarczyńska E, Brański P, Szewczyk B, Wierońska JM, Kłak K, Chojnacka-Wójcik E, Nowak G, Pilc A (2004) Group III mGlu receptor agonists produce anxiolytic- and antidepressant-like effects after central administration in rats. Neuropharmacology 46:151–159.

Penzo MA, et al. (2015) The paraventricular thalamus controls a central amygdala fear circuit. Nature 519:455.

Perlman G, Tanti A, Mechawar N (2021) Parvalbumin interneuron alterations in stress-related mood disorders: a systematic review. Neurobiol Stress 15:100380.

Pettitt SJ, Liang Q, Rairdan XY, Moran JL, Prosser HM, Beier DR, Lloyd KC, Bradley A, Skarnes WC (2009) Agouti C57BL/6N embryonic stem cells for mouse genetic resources. Nat Methods 6:493–495.

Pratt JA, Morris BJ (2015) The thalamic reticular nucleus: a functional hub for thalamocortical network dysfunction in schizophrenia and a target for drug discovery. J Psychopharmacol 29:127–137.

Raber J, Duvoisin RM (2015) Novel metabotropic glutamate receptor 4 and glutamate receptor 8 therapeutics for the treatment of anxiety. Expert Opin Investig Drugs 24:519–528.

Radovanovic L, Petrovic J, Saponjic J (2021) Hippocampal and reticulothalamic parvalbumin interneurons and synaptic re-organization during sleep disorders in the rat models of Parkinson's disease neuropathology. Int J Mol Sci 22:1.

Robbins MJ, et al. (2007) Evaluation of the mGlu8 receptor as a putative therapeutic target in schizophrenia. Brain Res 1152:215–227.

Salimando GJ, Hyun M, Boyt KM, Winder DG (2020) BNST GluN2D-containing NMDA receptors influence anxiety- & depressive-like behaviors and modulate cell-specific excitatory/inhibitory synaptic balance. J Neurosci 40:3949–3968.

Saugstad JA, Kinzie JM, Shinohara MM, Segerson TP, Westbrook GL (1997) Cloning and expression of rat metabotropic glutamate receptor 8 reveals a distinct pharmacological profile. Mol Pharmacol 51:119–125.

Skarnes WC, et al. (2011) A conditional knockout resource for the genome-wide study of mouse gene function. Nature 474:337–344.

Spooren W, Lesage A, Lavreysen H, Gasparini F, Steckler T (2010) Metabotropic glutamate receptors: their therapeutic potential in anxiety. Curr Top Behav Neurosci 2:391–413.

Steullet P, Cabungcal JH, Bukhari SA, Ardelt MI, Pantazopoulos H, Hamati F, Salt TE, Cuenod M, Do KQ, Berretta S (2018) The thalamic reticular nucleus in schizophrenia and bipolar disorder: role of parvalbumin-expressing neuron networks and oxidative stress. Mol Psychiatry 23:2057–2065.

Terracciano A, et al. (2010) Genome-wide association scan of trait depression. Biol Psychiatry 68:811–817.

Thankachan S, et al. (2019) Thalamic reticular nucleus parvalbumin neurons regulate sleep spindles and electrophysiological aspects of schizophrenia in mice. Sci Rep 9:3607.

Wang S, Bickford ME, Van Horn SC, Erisir A, Godwin DW, Sherman SM (2001) Synaptic targets of thalamic reticular nucleus terminals in the visual thalamus of the cat. J Comp Neurol 440:321–341.

Wells MF, Wimmer RD, Schmitt LI, Feng G, Halassa MM (2016) Thalamic reticular impairment underliesattention deficit in Ptchd1Y/− mice. Nature 532:58.

White JK, et al. (2013) Genome-wide generation and systematic phenotyping of knockout mice reveals new roles for many genes. Cell 154:452.

You QL, Luo ZC, Luo ZY, Kong Y, Li ZL, Yang JM, Li XW, Gao TM (2021) Involvement of the thalamic reticular nucleus in prepulse inhibition of acoustic startle. Transl Psychiatry 11:241.

Zhu X, Cabungcal JH, Cuenod M, Uliana DL, Do KQ, Grace AA (2021) Thalamic reticular nucleus impairments and abnormal prefrontal control of dopamine system in a developmental model of schizophrenia: prevention by *N*-acetylcysteine. Mol Psychiatry 26:7679–7689.

Zhu YB, Wang Y, Hua XX, Xu L, Liu MZ, Zhang R, Liu PF, Li JB, Zhang L, Mu D (2022) PBN-PVT projections modulate negative affective states in mice. Elife 11:e68372.

Zikopoulos B, Barbas H (n.d.) Circuits for multisensory integration and attentional modulation through the prefrontal cortex and the thalamic reticular nucleus in primates.